

Parallel finite element computation of free-surface flows

I. Güler, M. Behr, T. Tezduyar

117

Abstract In this paper we present parallel 2D and 3D finite element computation of unsteady, incompressible free-surface flows. The computations are based on the Deformable-Spatial-Domain/Stabilized Space-Time (DSD/SST) finite element formulation, which takes automatically into account the motion of the free surface. The free-surface height is governed by a kinematic free-surface condition, which is also solved with a stabilized formulation. The meshes consist of triangles in 2D and triangular-based prism elements in 3D. The mesh update is achieved with general or special-purpose mesh moving schemes. As examples, 2D flow past spillway of a dam and 3D flow past a surface-piercing circular cylinder are presented.

1 Introduction

Free-surface flow problems involve spatial domains which change their shapes due to the motion of the free surface. The location of the free surface is not known a priori and is determined as part of the overall solution. This leads to a geometric nonlinearity in addition to the nonlinearities that are already part of the Navier-Stokes equations.

The Deformable-Spatial-Domain/Stabilized Space-Time (DSD/SST) finite element formulation was first introduced in Tezduyar et al. (1992a) and Tezduyar et al. (1992b), and was applied to many classes of flow problems involving moving boundaries and interfaces (see e.g. Tezduyar et al. 1996). In this approach, the stabilized finite element formulations of the governing equations are written over the space-time domain of the problem. With this, changes in

the shape of the spatial domain due to the motion of the boundaries and interfaces are taken into account automatically. This approach gives us the capability to solve a large class of problems, such as free surfaces, two-fluid interfaces and fluid-structure interactions.

The standard Galerkin formulation of incompressible flows can involve two well-known numerical instabilities. The first one is due to the presence of advection terms in the governing equations. The second numerical instability is unique to mixed methods and is caused by using unacceptable combinations of interpolation functions to represent the velocity and pressure fields. In the work reported here, the DSD/SST formulation is based on stabilization of the method with the Galerkin/least-squares approach. The finite element functions are linear both in space and time, continuous in space, but discontinuous in time. This discontinuity in time allows the computations to be carried out one space-time “slab” at a time, where the “slab” is a slice of the space-time domain between two consecutive time levels. It also gives us the option of changing the spatial discretization from one time step to another.

In the DSD/SST formulation, a large, coupled system of nonlinear equations needs to be solved at every time step of the simulation. These systems are solved with Newton-Raphson iterations. Each step of the Newton-Raphson sequence requires the solution of a linear equation system. These systems are also solved iteratively, using the GMRES technique (Saad and Schultz 1986).

In Sect. 2, we review the Navier-Stokes equations of incompressible flows and describe the turbulence model. The stabilized finite element formulations are presented in Sect. 3. The mesh update method is discussed in Sect. 4. The issues concerning moving contact line and outflow boundary condition are addressed in Sect. 5 and 6, respectively. The elements used, especially the triangular-based prisms, are discussed in Sect. 7. In Section 8, we report simulation of 2D flow past spillway of a dam and 3D flow past a surface-piercing circular cylinder. We provide our concluding remarks in Sect. 9.

2 Governing equations

The computations are based on solution of the time-dependent Navier-Stokes equations of incompressible flows. We consider a viscous, incompressible fluid occupying at an instant $t \in (0, T)$ a bounded region $\Omega_t \subset \mathbb{R}^{n_{sd}}$, with boundary Γ_t , where n_{sd} is the number of space dimensions. In the DSD/SST formulation, the spatial domain may change with respect to time, and the subscript t in-

I. Güler, M. Behr
Army HPC Research Center, 1100 Washington Avenue South,
Minneapolis, MN 55415, USA

T. Tezduyar
Army HPC Research Center,
Mechanical Engineering and Material Science,
Rice University-MS 321, 6100 Main Street,
Houston, TX 77005, USA
<http://www.memr.rice.edu/TAFSM>

Correspondence to: T. Tezduyar

This work was sponsored by the Army High Performance Computing Research Center under the auspices of the Department of the Army, Army Research Laboratory cooperative agreement number DAAH04-95-2-0003/contract number DAAH04-95-C-0008. The content does not necessarily reflect the position or the policy of the Government, and no official endorsement should be inferred.

icates such time-dependence. The symbols $\mathbf{u}(\mathbf{x}, t)$ and $p(\mathbf{x}, t)$ represent the velocity and pressure. The external forces (e.g., the gravity) are represented by $\mathbf{f}(\mathbf{x}, t)$. The momentum and mass balance equations can be written as follows:

$$\rho \left(\frac{\partial \mathbf{u}}{\partial t} + \mathbf{u} \cdot \nabla \mathbf{u} - \mathbf{f} \right) - \nabla \cdot \boldsymbol{\sigma} = 0 \text{ on } \Omega_t \quad \forall t \in (0, T), \quad (1)$$

$$\nabla \cdot \mathbf{u} = 0 \text{ on } \Omega_t \quad \forall t \in (0, T), \quad (2)$$

where the density ρ is assumed to be constant. The stress tensor $\boldsymbol{\sigma}$ can be decomposed into its isotropic and deviatoric parts:

$$\boldsymbol{\sigma}(\mathbf{u}, p) = -p\mathbf{I} + \mathbf{T}. \quad (3)$$

We consider only the Newtonian fluids, for which the deviatoric stress is related linearly to the strain rate tensor:

$$\mathbf{T} = 2\mu\boldsymbol{\varepsilon}(\mathbf{u}), \quad \boldsymbol{\varepsilon}(\mathbf{u}) = \frac{1}{2} \left(\nabla \mathbf{u} + (\nabla \mathbf{u})^T \right), \quad (4)$$

where μ is the dynamic viscosity. The Dirichlet and Neumann-type boundary conditions are represented as

$$\mathbf{u} = \mathbf{g} \quad \text{on } (\Gamma_t)_g, \quad (5)$$

$$\mathbf{n} \cdot \boldsymbol{\sigma} = \mathbf{h} \quad \text{on } (\Gamma_t)_h, \quad (6)$$

where $(\Gamma_t)_g$ and $(\Gamma_t)_h$ are complementary subsets of the boundary Γ_t .

Boundary conditions imposed on the free surface consist of kinematic and dynamic conditions. The kinematic condition requires that the free surface is a material surface; i.e. the fluid particles which are at some time on the free surface always stay on it. This condition is used to describe the motion of the free surface. For a 3D problem, on the free-surface $z = H(x, y, t)$,

$$\frac{\partial H}{\partial t} + u_s \frac{\partial H}{\partial x} + v_s \frac{\partial H}{\partial y} - w_s = 0 \quad \text{on } S \quad \forall t \in (0, T), \quad (7)$$

where H is the free-surface elevation and the subscript s refers to quantities at the free surface. The domain S is the lower-dimensional region over which H is determined, typically obtained from Ω_t by projection. The surface tension effects are neglected, and the stress-free condition is imposed as the dynamic condition on the free surface.

The initial condition consists of a divergence-free velocity field specified over the entire domain:

$$\mathbf{u}(\mathbf{x}, 0) = \mathbf{u}_0, \quad \nabla \cdot \mathbf{u}_0 = 0 \quad \text{on } \Omega_0. \quad (8)$$

In the present study, there are two dimensionless parameters that characterize the flow. They are the Reynolds number:

$$\text{Re} = \frac{\rho UL}{\mu}, \quad (9)$$

which is the ratio of inertial forces to viscous forces; and the Froude number:

$$\text{Fr} = \frac{U}{\sqrt{gL}}, \quad (10)$$

which is the ratio of inertial forces to gravity forces. In these definitions, U and L denote characteristic velocity and length, respectively.

Because the typical meshes are not able to resolve the flow features well enough to fully capture turbulence effects at high Reynolds numbers, introduction of a turbulence model becomes necessary. In the present study, a simple Smagorinsky turbulence model is employed. In this model, the kinematic viscosity ν is augmented by an eddy viscosity ν_t which is defined as

$$\nu_t = (Ch)^2 (2\boldsymbol{\varepsilon}(\mathbf{u}) : \boldsymbol{\varepsilon}(\mathbf{u}))^{\frac{1}{2}}, \quad (11)$$

where C is a constant and h is the element length defined here as the maximum of the edge lengths for the element. Here, we set C to 0.15.

3 Stabilized finite element formulations

The computations are based on the space-time finite element method, in which the weak form of the governing equations is written over the associated space-time domain of the problem. To construct the finite element function spaces for the space-time method we partition the time interval $(0, T)$ into subintervals $I_n = (t_n, t_{n+1})$, where t_n and t_{n+1} belong to an ordered series of time levels $0 = t_0 < t_1 < \dots < t_N = T$. Let $\Omega_n = \Omega_{t_n}$ and $\Gamma_n = \Gamma_{t_n}$. We will define the space-time slab Q_n as the domain enclosed by the surfaces Ω_n , Ω_{n+1} , and P_n , where P_n is the surface described by the boundary Γ_t as t traverses I_n . As it is the case with Γ_t , surface P_n is decomposed into $(P_n)_g$ and $(P_n)_h$ with respect to the type of boundary condition (Dirichlet and Neumann) being applied.

For each space-time slab Q_n , we define the following finite-dimensional trial solution ($(\mathcal{S}_u^h)_n$ and $(\mathcal{S}_p^h)_n$) and test function ($(\mathcal{V}_u^h)_n$ and $(\mathcal{V}_p^h)_n$) spaces for the velocity and pressure:

$$(\mathcal{S}_u^h)_n = \left\{ \mathbf{u}^h \mid \mathbf{u}^h \in [H^{1h}(Q_n)]^{n_{sd}}, \quad \mathbf{u}^h \dot{=} \mathbf{g}^h \quad \text{on } (P_n)_g \right\}, \quad (12)$$

$$(\mathcal{V}_u^h)_n = \left\{ \mathbf{w}^h \mid \mathbf{w}^h \in [H^{1h}(Q_n)]^{n_{sd}}, \quad \mathbf{w}^h \dot{=} \mathbf{0} \quad \text{on } (P_n)_g \right\}, \quad (13)$$

$$(\mathcal{S}_p^h)_n = (\mathcal{V}_p^h)_n = \{p^h \mid p^h \in H^{1h}(Q_n)\}, \quad (14)$$

where $H^{1h}(Q_n)$ represents the finite-dimensional function space constructed over the space-time slab Q_n by using first-order polynomials in space and in time. The interpolation function spaces are discontinuous in time and continuous in space.

The stabilized space-time formulation of Eqs. (1) and (2) can then be written as follows: given $(\mathbf{u}^h)_n^-$, find $\mathbf{u}^h \in (\mathcal{S}_u^h)_n$ and $p^h \in (\mathcal{S}_p^h)_n$ such that $\forall \mathbf{w}^h \in (\mathcal{V}_u^h)_n$ and $\forall q^h \in (\mathcal{V}_p^h)_n$:

$$\begin{aligned}
& \int_{Q_n} \mathbf{w}^h \cdot \rho \left(\frac{\partial \mathbf{u}^h}{\partial t} + \mathbf{u}^h \cdot \nabla \mathbf{u}^h - \mathbf{f} \right) dQ \\
& + \int_{Q_n} \boldsymbol{\varepsilon}(\mathbf{w}^h) : \boldsymbol{\sigma}(\mathbf{u}^h, p^h) dQ + \int_{Q_n} q^h \nabla \cdot \mathbf{u}^h dQ \\
& + \int_{\Omega_n} (\mathbf{w}^h)_n^+ \cdot \rho \left((\mathbf{u}^h)_n^+ - (\mathbf{u}^h)_n^- \right) d\Omega \\
& + \sum_{e=1}^{(n_{el})_n} \int_{Q_n^e} \tau_{\text{MOM}} \frac{1}{\rho} \\
& \cdot \left[\rho \left(\frac{\partial \mathbf{w}^h}{\partial t} + \mathbf{u}^h \cdot \nabla \mathbf{w}^h \right) - \nabla \cdot \boldsymbol{\sigma}(\mathbf{w}^h, q^h) \right] \\
& \cdot \left[\rho \left(\frac{\partial \mathbf{u}^h}{\partial t} + \mathbf{u}^h \cdot \nabla \mathbf{u}^h - \mathbf{f} \right) - \nabla \cdot \boldsymbol{\sigma}(\mathbf{u}^h, p^h) \right] dQ \\
& + \sum_{e=1}^{(n_{el})_n} \int_{Q_n^e} \tau_{\text{CONT}} \nabla \cdot \mathbf{w}^h \rho \nabla \cdot \mathbf{u}^h dQ \\
& = \int_{(P_n)_h} \mathbf{w}^h \cdot \mathbf{h}^h dP . \tag{15}
\end{aligned}$$

The following notation is being used in Eq. (15):

$$(\mathbf{u}^h)_n^\pm = \lim_{\varepsilon \rightarrow 0} \mathbf{u}(t_n \pm \varepsilon) , \tag{16}$$

$$\int_{Q_n} \dots dQ = \int_{I_n} \int_{\Omega_t^h} \dots d\Omega dt , \tag{17}$$

$$\int_{P_n} \dots dP = \int_{I_n} \int_{\Gamma_t^h} \dots d\Gamma dt . \tag{18}$$

The definitions of the stabilization parameters τ_{MOM} and τ_{CONT} can be found in Behr and Tezduyar (1994).

The solution to Eq. (15) is obtained for all of the space-time slabs Q_0, Q_1, \dots, Q_{N-1} sequentially, and the computations start with

$$(\mathbf{u}^h)_0^- = \mathbf{u}_0^h . \tag{19}$$

The stabilized finite-element formulation of Eq. (7) can be written as

$$\begin{aligned}
& \int_S \psi^h \left(\frac{\partial H^h}{\partial t} + u_s^h \frac{\partial H^h}{\partial x} + v_s^h \frac{\partial H^h}{\partial y} - w_s^h \right) dS \\
& + \sum_{e=1}^{n_{el}} \int_{S^e} \tau_{\text{DC}} \left(\frac{\partial \psi^h}{\partial x} \frac{\partial H^h}{\partial x} + \frac{\partial \psi^h}{\partial y} \frac{\partial H^h}{\partial y} \right) dS \\
& + \sum_{e=1}^{n_{el}} \int_{S^e} \tau_{\text{SUPG}} \left(u_s^h \frac{\partial \psi^h}{\partial x} + v_s^h \frac{\partial \psi^h}{\partial y} \right) \\
& \cdot \left(\frac{\partial H^h}{\partial t} + u_s^h \frac{\partial H^h}{\partial x} + v_s^h \frac{\partial H^h}{\partial y} - w_s^h \right) dS = 0 . \tag{20}
\end{aligned}$$

The stabilization parameter for the discontinuity-capturing term can be defined as

$$\tau_{\text{DC}} = Ch_s^2 r(H^h) , \tag{21}$$

$$r(H) = \frac{\left| \frac{\partial H}{\partial t} + u_s^h \frac{\partial H}{\partial x} + v_s^h \frac{\partial H}{\partial y} - w_s^h \right|}{\max H - \min H} , \tag{22}$$

or, alternatively, as

$$\tau_{\text{DC}} = CUh_s , \tag{23}$$

where C is typically set to 1. The U in Eq. (23) represents reference velocity. The ‘‘artificial diffusion’’ form of the coefficient (23) is intended to be used only as a transitional measure, allowing the simulation to continue through dramatic surface deformations encountered during the initial stages. As the free surface stabilizes, more accurate transient behavior can be obtained using the consistent form (21).

The stabilization parameter for the SUPG term has the standard form:

$$\tau_{\text{SUPG}} = \frac{h_s}{2|\mathbf{u}_s|} , \tag{24}$$

where h_s is a measure of the element length.

Both of the nonlinear systems given by Eqs. (15) and (20) are solved with the Newton-Raphson method. The solution of flow variables and free surface updates are carried out in succession within the nonlinear iteration. This formulation has been implemented on parallel architectures, under data parallel model using Connection Machine Fortran (See Kennedy et al. 1994), and under message passing model using MPI library (See Tezduyar et al. 1996).

4 Mesh update method

In computation of free-surface flows with an interface-tracking technique, one needs to handle the changing spatial domain by updating the mesh. Two main update approaches can be employed for this purpose. The first one is based on moving the nodal points of the mesh. The second one is based on remeshing (i.e. generating a new set of nodes and elements). These two approaches can be used alone or in combination. The motion of the nodal points will be subject to boundary conditions conforming to the motion of the free surface. The motion of the free-surface is determined at every nonlinear iteration by solving the equation governing the free-surface height.

Once the new location of the free surface is known, we can use two different methods to determine the motion of the nodal points. One approach is to employ an automatic mesh moving scheme (Johnson and Tezduyar 1994). In this method, the modified equations of linear elasticity are solved using the finite element method to determine the internal nodal displacements. We can combine automatic mesh moving with remeshing as needed. Generation of the starting mesh and remeshing are typically accomplished by using an automatic mesh generator. The automatic mesh moving technique is used in the 2D example presented later in this paper.

Another approach is to use a special-purpose mesh moving scheme, typically in conjunction with a special-purpose mesh generator, to specify the motion of the mesh based on some pre-defined rules. This approach can be employed only in cases where the changes in the shape of the spatial domain is sufficiently simple. An earlier example, parallel 3D computation of sloshing in a vertically vibrating container, can be found in Behr and Tezduyar (1994).

In the 3D free-surface flow problem presented in Sect. 8.2, we move the nodal points only in the vertical direction. Once the new location of the free surface is calculated, the nodes are redistributed along the vertical lines according to a geometric progression rule. By doing so, we place the smaller elements near the free surface. An advantage of this method over the automatic mesh moving scheme is that we don't need to solve an additional equation system to update the mesh at every nonlinear iteration.

5

Moving contact line

In computation of free-surface flow past a solid object, special attention needs to be paid to handling a contact line where the free surface intersects the solid boundary. Imposing no-slip condition at the contact line gives rise to a stress singularity there. To circumvent this problem, the no-slip condition needs to be relaxed. This can be achieved by employing Navier's slip condition (Navier 1823) that makes the tangential components of stress at the solid surface proportional to the local slip velocity:

$$(\mathbf{I} - \mathbf{nn}) \cdot (\mathbf{n} \cdot \boldsymbol{\sigma}) = -\frac{1}{\beta} (\mathbf{I} - \mathbf{nn}) \cdot (\mathbf{u} - \mathbf{v}), \quad (25)$$

where \mathbf{u} is the velocity of the fluid, \mathbf{v} is the velocity of the solid object and β is an empirical slip coefficient. The \mathbf{n} represents the unit normal to the surface, and consequently, $\mathbf{I} - \mathbf{nn}$ is a geometric tensor which projects vectors onto the plane tangent to this surface. The no-slip ($\beta = 0$) and perfect slip ($\beta \rightarrow \infty$) conditions can be obtained as the limiting cases. In the 3D example reported in this paper, we use perfect slip condition on the surface-piercing body.

6

Outflow boundary condition

In computation of the Navier-Stokes equations, the computational domain needs to be truncated to a finite size. The conditions imposed at the boundaries of the computational domain are typically in the form of inflow or outflow conditions. These boundary conditions must be chosen carefully enough to obtain realistic solutions. It is a common practice to specify the velocity profile at an inflow boundary. At an outflow boundary, on the other hand, the choice is not as clear. Often one seeks an outflow boundary condition that allows the flow to exit the domain with the least influence on the upstream regions. In the absence of a body force field (e.g. a gravitational field), one can use a stress-free boundary condition. However, the stress at the outflow boundary is not zero for free-surface flows, and the contributions coming from the boundary integral term on the right-hand side of Eq. (15) have to be taken into account. In the 3D simulation of free-surface flows which involves an artificial outflow boundary, we use the "free boundary condition" of Papanastasiou et al. (1992). The free boundary condition can be described as imposing no boundary condition at all. Therefore it is also called "no boundary condition outflow boundary condition". In this boundary condition, the validity of weighted

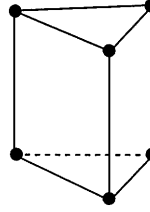


Fig. 1. A triangular-based prism element

residual momentum equation is extended to the outflow boundary, and the boundary integral is evaluated in terms of unknown values of the velocity and pressure.

To further eliminate the effects of possible artificial reflections from the outflow boundary, one can enlarge the computational domain by placing the outflow boundary far downstream, so that within a given time period the reflected waves do not reach the region of interest.

7

Triangular-based prism elements

In this study, we use meshes composed of triangular elements in the 2D case, and a mesh that consists of triangular-based prism elements (see Fig. 1) in the 3D case. The latter is structured in the vertical direction but it may be structured or unstructured in the horizontal plane. This allows the use of a special-purpose mesh moving scheme. Only the triangular faces of the prism elements lie on the free surface. This is advantageous because the abrupt changes in the free-surface elevation, e.g. hydraulic jumps, can be more easily handled by using triangular elements on the free surface.

8

Numerical examples

8.1

2D free-surface flow past spillway of a dam

This simulation complements our earlier 3D simulation of flow past the spillway of the Olmsted Dam on the Ohio River, reported in Tezduyar et al. (1996). This dam design is currently under study by the U.S. Army Corps of Engineers. This simulation is an example application of the DSD/SST formulation coupled with the elasticity-based automatic mesh update method, and a stabilized formulation of the equation governing the free-surface height.

The model represents a 500 ft-long section of the navigation pass, and includes a long upstream channel, the spillway crest, and the stilling basin. The initial mesh consists of 7966 space-time nodes and 7571 triangular elements. A flow rate of 271 cfs/ft is assumed, and the Reynolds number based on the upstream velocity and the spillway length is approximately 7×10^6 . The Froude number based on the upstream velocity and depth is 0.217. Starting with a flat water surface, the flow is computed for 185 time steps with a time step size of 0.1 s, with the discontinuity-capturing coefficient as defined by Eq. (21), until large mesh deformations force us to remesh. Frames from this initial part of the simulation are shown in Figs. 2 and 3, displaying the deforming mesh and the velocity field. After remeshing, the flow is computed for another

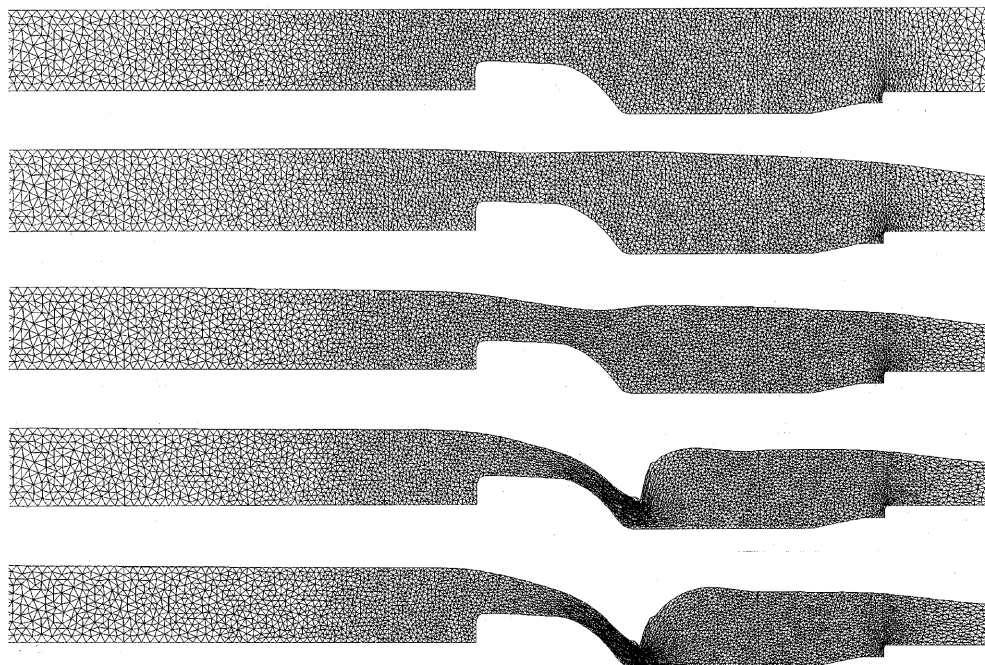


Fig. 2. 2D free-surface flow past spillway of a dam: mesh at $t = 0, 5, 10, 15$ and 18 s

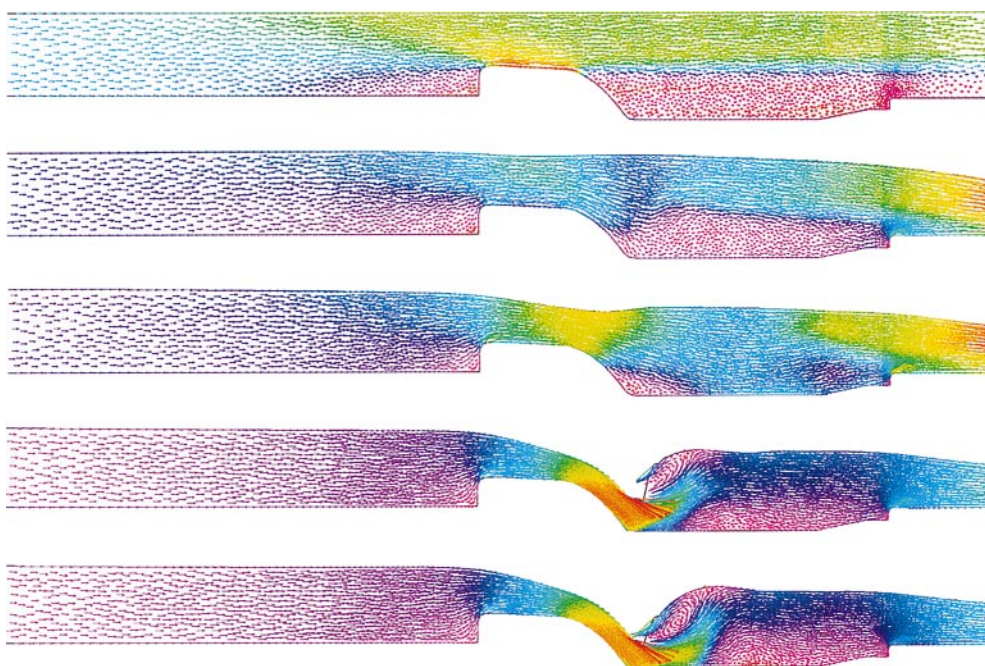


Fig. 3. 2D free-surface flow past spillway of a dam: velocity field at $t = 0, 5, 10, 15$ and 18 s

2000 time steps with a time step size of 0.025 s, using the discontinuity-capturing term as defined by Eq. (23). The flow eventually reaches a time-periodic state. The frames from this part of the simulation are shown in Figs. 4 and 5.

This simulation is part of a collaborative project with R. Stockstill and C. Berger at the Waterways Experiment Station. The computation was carried out on a CRAY T3D.

8.2 3D free-surface flow past a circular cylinder

In this problem, free-surface flow past a circular cylinder is simulated. The cylinder stands vertically and penetrates

the free surface. The Reynolds number based on the upstream velocity and cylinder diameter is 1×10^7 . The upstream Froude number is 0.564. The surface height at the upstream and the velocity profile at the inflow boundary are specified. Perfect slip condition is imposed on the cylinder surface. At the side and bottom boundaries the tangential components of the stress and the normal component of the velocity are set to zero. The mesh consists of 230,480 triangular-based prism elements and 258,764 space-time nodes; it is shown in Figs. 6 and 7. The computation was carried out on the Thinking Machines CM-5.

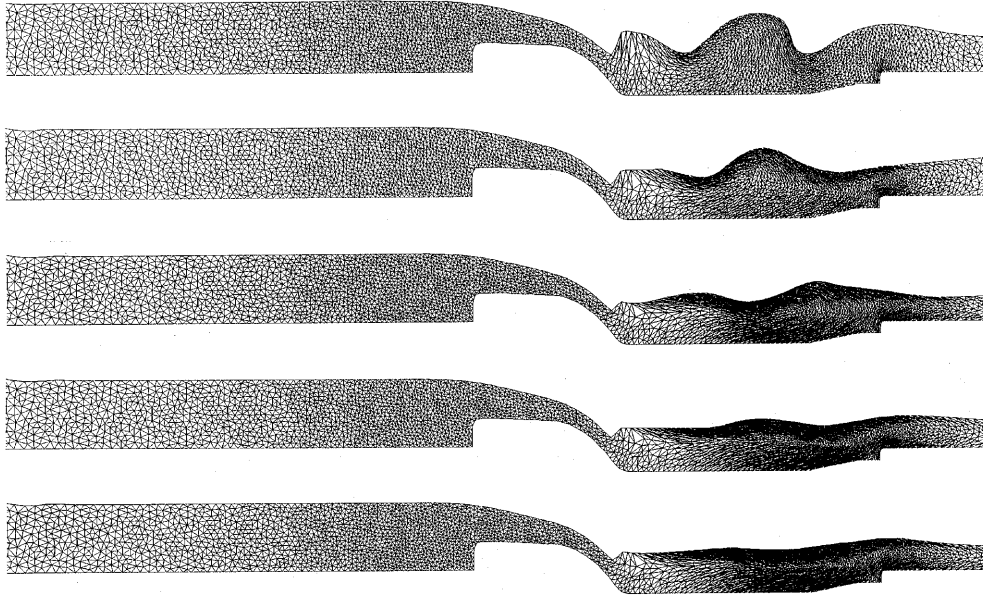


Fig. 4. 2D free-surface flow past spillway of a dam: mesh at $t = 25, 35, 45, 55$ and 65 s

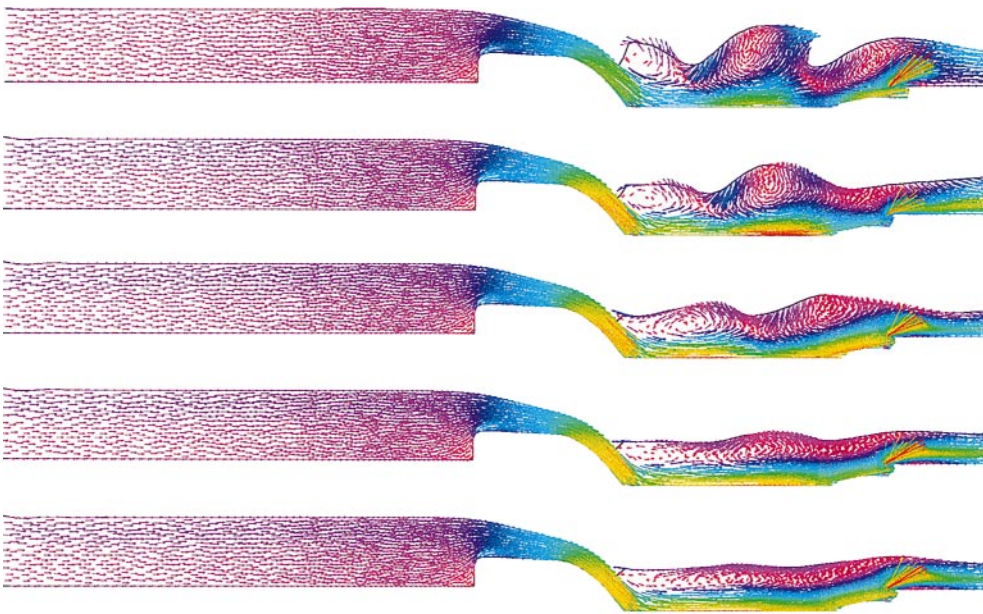


Fig. 5. 2D free-surface flow past spillway of a dam: velocity field at $t = 25, 35, 45, 55$ and 65 s

Figure 8 shows the free-surface mesh at an instant. Figure 9 shows the computed wave patterns close to the cylinder. Here, the free surface is color-coded with the

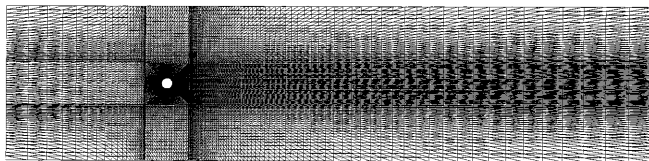


Fig. 6. 3D free-surface flow past a circular cylinder: mesh in the x - y plane



Fig. 7. 3D free-surface flow past a circular cylinder: mesh in the x - z plane

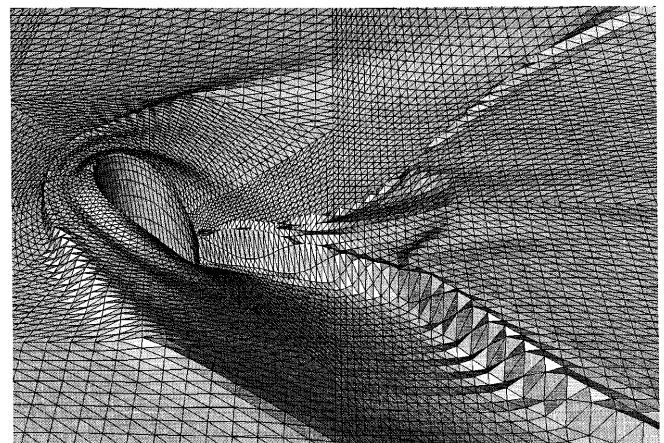


Fig. 8. 3D free-surface flow past a circular cylinder: free-surface mesh near the cylinder at an instant

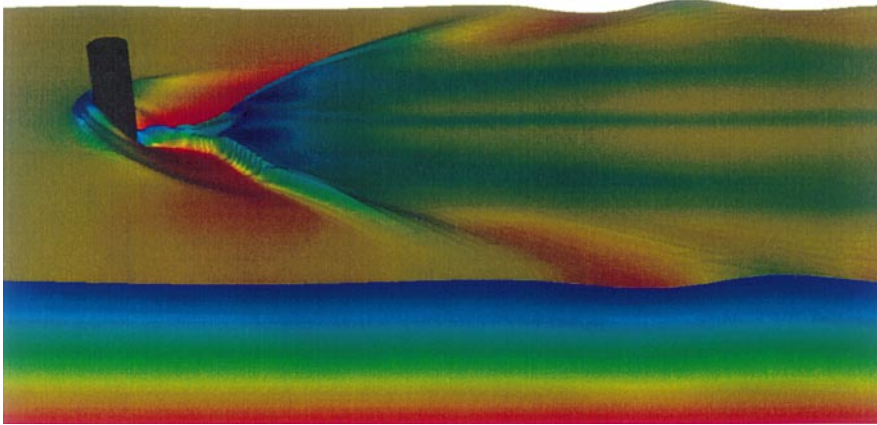


Fig. 9. 3D free-surface flow past a circular cylinder: computed wave patterns at an instant

velocity magnitude, and the side boundary is color-coded with the fluid pressure. In the vertical plane of symmetry, the flow comes to rest at the upstream face of the cylinder. Since the flow decelerates in this region, the static pressure increases and as a result the water level rises; i.e. a bow wave forms in front of the cylinder. Then, the flow accelerates as it goes around the cylinder. This results in a corresponding decrease in the static pressure and a rapid lowering of the water surface is observed; i.e. a hollow forms behind the cylinder. In addition, an oblique hydraulic jump is observed at the cylinder wake. This is in the form of an abrupt increase in the free-surface height and turns the deflected flow to the streamwise direction.

9 Concluding remarks

We presented methods for parallel finite element computation of unsteady incompressible flows with free surfaces. Our computations are based on the Deformable-Spatial-Domain/Stabilized Space-Time (DSD/SST) finite element formulation that automatically takes into account the motion of the free surface. The free-surface height is governed by a kinematic free-surface condition, which is solved also with a stabilized formulation. The meshes used consist of triangular elements in 2D and triangular-based prism elements in 3D. The mesh update is achieved with general- or special-purpose mesh moving schemes. As examples, 2D flow past spillway of a dam and 3D flow past a circular cylinder were presented.

References

- Behr M, Tezduyar TE** (1994) Finite element solution strategies for large-scale flow simulations. *Comp. Meth. Appl. Mech. Eng.* 112:3–24
- Johnson AA, Tezduyar TE** (1994) Mesh update strategies in parallel finite element computations of flow problems with moving boundaries and interfaces. *Comp. Meth. Appl. Mech. Eng.* 119:73–94
- Kennedy JG, Behr M, Kalro V, Tezduyar TE** (1994) Implementation of implicit finite element methods for incompressible flows on the CM-5. *Comp. Meth. Appl. Mech. Eng.* 119:95–111
- Navier CLMH** (1823) Sur les lois du mouvement des fluides. *Memoires de l'Académie royale des Sciences de l'Institut de France*, 6:389–440
- Papanastasiou TC, Malamataris N, Ellwood K** (1992) A new outflow boundary condition. *Int. J. Num. Meth. Fluids* 14:587–608
- Saad Y, Schultz M** (1986) GMRES: A generalized minimal residual algorithm for solving nonsymmetric linear systems. *SIAM Journal of Scientific and Statistical Computing* 7:856–869
- Tezduyar TE, Aliabadi S, Behr M, Johnson A, Kalro V, Litke M** (1996) Flow simulation and high performance computing. *Comput. Mech.* 18:397–412
- Tezduyar TE, Behr M, Liou J** (1992a) A new strategy for finite element computations involving moving boundaries and interfaces – the deforming-spatial-domain/space-time procedure: I. The concept and the preliminary tests. *Comp. Meth. Appl. Mech. Eng.* 94:339–351
- Tezduyar TE, Behr M, Mittal S, Liou J** (1992b) A new strategy for finite element computations involving moving boundaries and interfaces – the deforming-spatial-domain/space-time procedure: II. Computation of free-surface flows, two-liquid flows, and flows with drifting cylinders. *Comp. Meth. Appl. Mech. Eng.* 94:353–371